

The Stress Field in the Northern Apulia (Southern Italy), as Deduced from Microearthquake Focal Mechanisms: New Insight from Local Seismic Monitoring

Marilena Filippucci(✉), Pierpaolo Pierri, Salvatore de Lorenzo, and Andrea Tallarico

Università degli Studi di Bari Aldo Moro, Dipartimento di Scienze della Terra e Geoambientali, Campus Universitario, via E. Orabona n°4, 70125 Bari, Italy
marilena.filippucci@uniba.it

Abstract. The historical seismicity catalogs report that the Gargano area (Apulia region, southern Italy) has been site of medium to high magnitude earthquakes. Instrumental seismicity suffers of the poor coverage of the seismic stations of the RSN (National Seismic Network). To improve the seismological monitoring of the area, in 2013 the OTRIONS seismic network (OSN), managed by the University of Bari - Italy, in cooperation with INGV (National Institute of Geophysics and Volcanology), was installed. In this study, focal mechanisms of single and composite events have been computed using 118 micro-earthquakes occurred in this area. We subdivided the dataset into subsets according to their location and depth, distinguishing between the Promontory zone and the Apulian foredeep. High quality focal mechanisms and low-misfit stress tensor inversion were obtained for three groups of events. To better constrain the stress tensor we included also focal mechanism solutions obtained in previous studies. In the southwestern Apulian foredeep zone, a normal fault kinematics is inferred, normal to the Apennine stress direction; in the Promontory zone, the fault kinematics indicate inverse fault mechanisms striking in NE-SW direction. Differently from previous analyses, the stress orientations inferred in this study agree with those inferred in the World Stress Map.

Keywords: Gargano promontory (Southern Italy) · Focal mechanisms · Stress tensor inversion · Microseismicity · OTRIONS seismic network

1 Introduction

The Apulia region (southern Italy) is presently characterized by low to moderate seismicity, as shown by the instrumental observations, while the historical catalogues report 15 earthquakes with $M_w > 5.5$ striking the Gargano promontory and surrounding area since 1361 (Rovida et al. 2019) (Fig. 1). The historical San Severo earthquake, occurred in 1627, is the most energetic earthquake in the area (Del Gaudio et al. 2007), even if the identification of the causative fault is still an open question. On the contrary, both the recent 2002 San Giuliano di Puglia earthquake and the 1893

© Springer Nature Switzerland AG 2020
O. Gervasi et al. (Eds.): ICCSA 2020, LNCS 12255, pp. 914–927, 2020.
https://doi.org/10.1007/978-3-030-58820-5_66

Mattinata earthquake are related to the activity along the E-W trending South Gargano fault line (Borre et al. 2003). In fact, it is generally accepted that the Molise earthquake is due to the reactivation of E-W striking faults (Di Bucci and Mazzoli 2003; Valensise et al. 2004) whose surface expression is probably represented by the E-W Mattinata fault (Fig. 1) in the Gargano Promontory (Tondi et al. 2005).

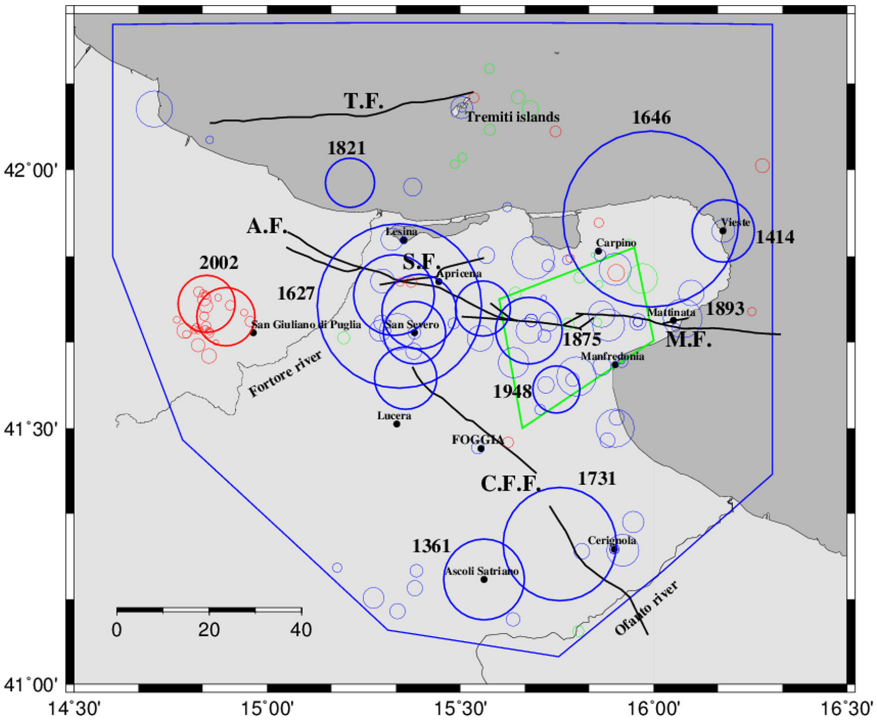


Fig. 1. Seismicity of northern Apulia extracted in the blue polygonal area from the CPTI2015 version 2.0 catalogue (Rovida et al. 2019). Circles represent focal volumes according to Bath and Duda (1964) formula: thicker ones correspond to events with $M_w \geq 5.5$: blue, green and red ones correspond to events occurred between 1361–1983, 1984–1999, 2000–2017, respectively. Noteworthy fault systems, proposed as possible seismogenic structures by authors cited in brackets, are shown with red lines: A.F. = Apricena fault (Patacca and Scandone, 2004), C.F. F. = Cerignola - Foggia fault (Patacca and Scandone, 2001), M.F. = Mattinata fault (Valensise et al., 2004), S.F. = Sannicandro Garganico - Apricena fault (Salvi et al., 1999), T.F. = Tremiti fault (Favali et al. 1993). The study area is marked by green line. (Color figure online)

Analyzing 10 years of seismicity (1995–2004), Milano et al. (2005) concluded that the E-W striking fault system in the Gargano Promontory presents a dextral slipping in response to a NW-SE compression, affecting the deeper layers of the crust, since the foci depths concentrate between 15 and 25 km. This behavior is interpreted as a geodynamic process consisting of the eastward rollback of the Adriatic foreland respect to the Apulian foreland that, causing a northeastward propagation of the thrust front of

Northern Apennines faster than that of Southern Apennines, determines the active dextral strike-slip tectonics on both the Gargano Promontory (Milano et al. 2005) and on the Tremiti Islands (Doglioni et al. 1994).

By analyzing the instrumental seismicity occurred between 1985 and 2004, Del Gaudio et al. (2007) tried to identify the seismogenic structures responsible of both the 1627 San Severo earthquake and the seismicity of the northern Apulia. The authors distinguished between foreland and foredeep regions: the first one is characterized by a regional stress combining NW compression and NE extension, so that seismogenic structures should be strike–slip faults (N-S sinistral or E-W dextral faults), with a slight transpressive character; the second one is characterized by transtensive mechanisms with NW oriented normal faults, similar to the dominant NE extension of the Apennine chain.

In the Gargano area, the local seismic network OTRIONS (hereafter OSN) revealed an intense seismic activity never recorded before, with magnitude less than that of the Apennine Chain.

In this paper we propose an evaluation of the stress field regime in the Gargano promontory, through a focal mechanism analysis of microearthquakes recorded by the OSN seismic network. We investigate the lateral and depth dependence of the stress field in the Gargano Promontory fault zone. Since about the 80% of the recorded earthquakes have magnitude smaller than 2, we carried out a preliminary manual refined picking of seismograms. Focal mechanisms for both the single and the composite event, were computed from the inversion of P wave polarities. Several tests were carried out by inverting different combinations of data. Finally, based on the obtained results and other observational evidence, a possible stress accumulation mechanism of the Gargano Promontory is proposed.

2 Data from the OTRIONS Seismic Network

The dataset considered in this paper is described by de Lorenzo et al. (2017). It consists of about 400 earthquakes localized in the Gargano Promontory and surrounding areas, occurring over a period of approximately 15 months (from April 2013 to July 2014). The events were recorded mainly by OSN and sporadically integrated by some stations belonging to the national seismic network of the INGV. Over 93% of the considered events were not detected by the INGV Earthquakes National Center (CNT). The maximum epicentral distances do not exceed 25 km and the magnitudes range from 0.1 to 1.7.

The considered earthquakes can be grouped into three categories according to the depth and geographical position of their hypocenter. Following the work of Filippucci et al. (2019a), we have analyzed the G1 group of events (blue circles in Fig. 2) among the events that fall within the area with the greatest surface heat flow density (ZSW area in Filippucci et al. 2019a), the G3 group of events (red circles in Fig. 2) that fall into the area with the lowest surface heat flow in the Gargano Promontory (ZNE area in Filippucci et al. 2019a) and a group of events (G2 group, yellow circles in Fig. 2) which fall into a “transition zone” between the ZSW and ZNE areas.

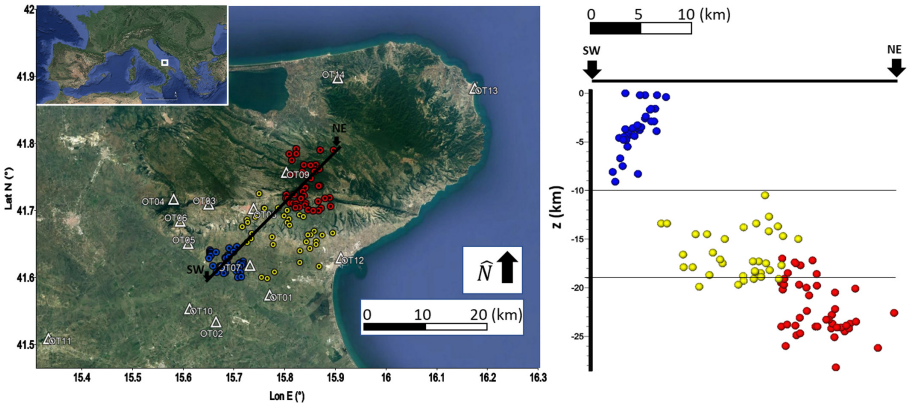


Fig. 2. Geographical map of the Gargano Promontory and depth distribution of earthquake foci along the black profile (SW-NE). The blue, red, yellow circles are the epicentres of the earthquakes of the group G1, G2, G3 respectively. The stations of the OTRIONS seismic network are reported as white triangles. (Color figure online)

Group G1. It consists of 38 events located in the area bounded between the Apulian foredeep and the Gargano foreland. The foci depth is rather shallow, between about 1 and 10 km, with an average depth of 3.8 km. The magnitudes are very small, ranging between 0.7 and 1.5 (average magnitude 1.0).

Group G2. It consists of 35 events with epicenters belonging to an area between the shallower (G1 group) and the deeper (G3 group) earthquakes. The foci depth ranges between 10 and 20 km with an average of 16.5 km. The magnitudes vary between 0.1 and 1.6 with an average of 0.8.

Group G3. It consists of 45 earthquakes which occurred inside the Gargano Promontory. The hypocentral depths range between 17 and 28 km, with an average of about 22 km. The magnitudes range between 0.3 and 1.7 (average magnitude 0.9).

The three identified groups of events were then used to derive the fault plane solutions of the Gargano micro-earthquakes as a function of the depth by moving along the SW-NE direction.

3 Single and Composite Fault Plane Solutions

The fault plane solutions were calculated using the FPFIT code (Reasenberg and Oppenheimer 1985). The velocity model used for the computation of the azimuths and the take-off angles is the same as that used for the location of events (de Lorenzo et al. 2017). We examined 118 earthquakes, 966 P-wave were picked, and 648 P-polarities were recognized. We discarded all the events for which less than 6 polarities were available allowing the inference of the fault plane solutions only for 58 micro-earthquakes. The remaining 60 events, characterized by a number of P polarities less than 6, were however used in the determination of the composite focal mechanism.

From the focal mechanism solutions, we selected the solutions based on the two FPFIT output quality factors Q_f and Q_p. All focal mechanisms with one or both quality factors C were rejected. Another useful parameter in the FPFIT inversion output is STDR, i.e. the station distribution ratio, that ranges inside {0.0,1.0} and sensitive to the distribution of the data on the focal sphere, relative to the radiation pattern. When STDR < 0.5 it means that a relatively large number of data fall too close to nodal planes; such a solution is less robust than one for which STDR > 0.5 and then it was rejected.

As discussed by Imanishi et al. (2011), P wave first-motion polarity alone cannot constrain the mechanism of earthquakes by using only few data. Since most of the events have magnitude less than 2, the number of P wave polarities ranges between 6 and 12. Although this is a high number of P polarities for events with this small size, it remains a low number for the purpose of constraining the fault plane solution. In order to better constrain to the FPFIT inversion, we attributed a weight to the polarity datum which varies from 0 to 2 (following the weighting of the picking used by SAC software). The attribution of the weights to the polarity data used in the FPFIT inversion lowers the misfit. The best fit solution of each event was determined by minimizing the residual between the observed and theoretical amplitudes, where a grid search approach was applied for strike, dip, and slip angles at 5° intervals. The next step was to obtain the composite focal mechanism for each identified group of events; the use of P polarities of grouped events allows to increase the coverage of the focal sphere under the hypothesis that the events of each group are attributable to an ideal single structure.

Group G1. For this group a total of 149 P-polarities was recognized among 264 identified P-wave arrival times. As concerns the single event solutions, 10 focal mechanism solutions were determined and 9 of them are constrained by data. Following the diagram of Zoback (1992), 3 of the 9 single focal mechanisms are of unknown (U) fault type and were discarded. The remaining 6 fault plane solutions are listed in Table 1 and plotted in Fig. 3 (locations in Appendix).

The composite focal mechanism was then obtained by performing two different inversions: the first by considering the polarity data of all the 38 earthquakes of the group; the second by considering only the 9 best single solutions. The results of the 2 obtained composite focal mechanism are very similar to each other (Table 4) and are classified as normal fault (NF) type (Fig. 3).

Group G2. For this group a total of 214 P-polarities was recognized among 298 P-wave arrival times. As concerns the single event solutions, 20 focal mechanism solutions were determined, with rather stable solutions. Three of these events were discarded because of the quality factors of type C, two events were discarded since STDR < 0.5. As a result of this data selection, 15 single focal mechanism solutions were finally classified as thrust fault (TF) type and one NF type (Table 2 and Fig. 3, locations in Appendix).

The composite focal mechanism, obtained using all the available 214 polarities of the 35 events, is of the TF type and it remains stable also considering only the 15 best solution events (Table 4, Fig. 3).

Group G3. For this group a total of 404 P-polarities was recognized among 285 P-wave arrival times. As concerns the single event solutions, 28 focal mechanisms were determined. After the data selection by the quality factors and the STDR criterion, 13

single focal mechanism solutions were constrained with the majority of the events of TF type and only few solutions classified as strike-slip (SS), NF type and 4 of the U type, which were rejected (Table 3 and Fig. 3, locations in Appendix).

When computing the composite fault plane solutions both using all the available polarities and also limiting the inversion to the best solution events (Table 4), the fault plane solution is quite stable, and classified as TF type (Fig. 3).

Table 1. List of fault plane solutions of the events of group G1. For each event the identification number (Id), strike φ, dip δ and rake λ of the 2 nodal planes, the trend and plunge of the P and T axes, the STDR, the quality factors (Q_f and Q_p) and the fault type (FT) are reported.

G1 (Id)	φ_1	δ_1	λ_1	φ_2	δ_2	λ_2	Trend P	Plunge P	Trend T	Plunge T	STDR	Q_f	Q_p	FT
8	260	85	-30	353	60	-174	212	24	310	17	0.87	A	B	SS
11	45	55	-90	225	35	-90	315	80	135	10	0.85	A	B	NF
13	40	60	-80	201	31	-107	335	73	123	14	0.62	A	B	NF
15	40	65	-140	290	54	-31	260	45	163	6	0.63	A	B	NS
24	55	70	-140	309	53	-25	278	42	178	11	0.71	A	B	NS
34	75	65	-120	309	38	-43	302	59	186	15	0.71	A	A	NF

Table 2. As the Table 1 for the events of group G2.

G2 (Id)	φ_1	δ_1	λ_1	φ_2	δ_2	λ_2	Trend P	Plunge P	Trend T	Plunge T	STDR	Q_f	Q_p	FT
2	125	65	100	282	27	70	208	19	55	68	0.84	A	B	TF
7	125	65	110	264	32	54	200	18	69	64	0.80	A	B	TF
11	115	60	120	246	41	49	184	10	74	62	0.78	A	B	TF
13	150	20	140	278	77	74	21	31	169	55	0.65	A	A	TF
17	145	45	100	311	46	80	48	0	141	83	0.63	A	A	TF
19	135	40	130	267	61	62	17	11	130	63	0.71	A	B	TF
20	110	25	150	228	78	68	335	29	112	52	0.83	A	B	TF
22	50	25	80	241	65	95	328	20	160	69	0.80	A	A	TF
23	90	45	110	243	48	71	346	2	83	76	0.75	A	B	TF
25	340	10	100	150	80	88	241	35	58	55	0.83	A	B	TF
30	140	20	130	278	75	77	19	29	170	58	0.77	A	B	TF
31	190	10	-90	10	80	-90	280	55	100	35	0.80	A	B	NF
32	40	60	90	220	30	90	130	15	310	75	0.71	A	B	TF
33	355	55	90	175	35	90	85	10	265	80	0.71	A	B	TF
34	160	40	110	315	53	74	56	7	173	76	0.71	A	A	TF

Table 3. As the Table 1 for the events of group G3.

G3 (Id)	φ_1	δ_1	λ_1	φ_2	δ_2	λ_2	Trend P	Plunge P	Trend T	Plunge T	STDR	Q_f	Q_p	FT
5	150	40	130	282	61	62	32	11	145	63	0.62	A	A	TF
9	30	20	120	178	73	80	277	27	73	61	0.88	A	B	TF
12	75	40	70	280	53	106	359	7	242	76	0.50	A	A	TF
14	115	45	140	236	63	53	352	10	97	55	0.83	A	B	TF
19	155	50	90	335	40	90	245	5	65	85	0.70	A	B	TF
24	80	45	130	210	57	57	323	7	66	62	0.80	A	B	TF
35	140	45	100	306	46	80	43	0	136	83	0.69	A	A	TF
41	100	60	70	316	36	121	204	13	329	68	0.61	A	A	TF
44	120	35	130	254	64	66	2	16	125	63	0.72	A	B	TF

We analyzed the effect of the velocity model on focal mechanism solutions; by using the Calcagnile and Panza (1980) velocity model retrieved for the Apulian lithosphere, used in the paper of Del Gaudio et al. (2007), we inferred some small variations, of the P and T-axes orientations, with respect to the above described results, only for few events of G1 group. This may be due to the shallow foci depth which gives rise to different values of take-off angles. No difference is obtained for G2 and G3 groups.

Table 4. List of composite fault plane solutions. The number of events (N_{ev}) used for the composite solution, the number of polarities (N_{pol}), strike φ, dip δ and rake λ of the 2 nodal planes, the trend and plunge of the P and T axes, the STDR, the quality factors (Q_f and Q_p) and the fault type (FT) are reported.

	N_{ev}	N_{Pol}	φ_1	δ_1	λ_1	φ_2	δ_2	λ_2	Trend P	Plunge P	Trend T	Plunge T	STDR	Q_f	Q_p	FT
G1	38	149	50	55	-130	286	51	-47	261	58	167	2	0.61	C	A	NF
	9	56	55	50	-120	277	48	-59	258	67	166	1	0.60	C	A	NF
G2	35	214	95	40	110	250	53	74	351	7	108	76	0.72	C	B	TF
	15	120	115	50	120	253	48	59	184	1	92	67	0.71	C	A	TF
G3	45	285	70	55	60	295	45	126	181	6	283	65	0.53	C	A	TF
	13	110	100	45	120	241	52	63	349	4	89	69	0.75	C	B	TF



Fig. 3. Map of the Gargano area with the accepted focal mechanism solutions. Colors of the beach ball correspond to the single event focal mechanism (black), composite focal mechanism for the G1 group (blue), composite focal mechanism for the G2 group (yellow), composite focal mechanism for the G3 group (red). (Color figure online)

4 Stress Field in the Gargano Area

We performed the stress inversion of the available focal mechanisms by using the FMSI (Focal Mechanism Stress Inversion) package by Gephart (1990). This inversion scheme provides accurate estimates of the stress tensor since it resolves four of the six independent components of the stress tensor. This method allows to obtain the three eigenvectors, i.e. the maximum, the minimum and the intermediate compressive principal stress axis directions (σ_1, σ_3 and σ_2), and one dimensionless parameter $R = (\sigma_2 - \sigma_1)/(\sigma_3 - \sigma_1)$ which, combining the magnitudes of the principal stresses, constrains the shape of the stress ellipsoid. The R value ranges from $R = 0$ ($\sigma_2 = \sigma_1$) to $R = 1$ ($\sigma_2 = \sigma_3$).

The inversion uses the dataset of fault orientation to determine the best-fitting values of the four stress parameters.

To better constrain the stress values obtained by the FMSI inversion, to each fault plane solution a weight was assigned. After several tests, we assigned to each datum the weigh $W = \sum W_i$ (the weights W_i are detailed in Table 5) that decreases with decreasing the quality factors and that increases with increasing the number of polarities.

Table 5. Weighting criteria assigned to the fault plane solution in the FMSI inversion.

	Q_f=A, Q_p=A	Q_f=B, Q_p=B	N_{pol}=6	N_{pol}={7,8}	N_{pol}={9,10}	$N_{pol} \geq 11$
W_i; i={ Q_f , Q_p , N_{pol} }	3	2	0	1	2	3

We applied the two acceptance criteria of the stress solutions as proposed by Lu et al. (1997). The first criterion requires that the 95% confidence regions of the maximum and minimum principal directions must not overlap to consider as acceptable the solution. The second criterion, which account for the degree of heterogeneity of the investigated medium, requires that the misfit angle has not to exceed 6°. Only if these criteria hold, the stress solution can be considered homogeneous and acceptable.

The stress tensor inversion was applied to all three groups of events, defined in the preceding section and the results are listed and plotted in Fig. 4 and described below.

G1 Group. The stress field was inferred from the inversion of the 9 best constrained fault plane solutions. The 95% confidence regions of the solution are very narrow and the misfit = 3.86° indicates homogeneity of the medium. The axis of maximum compression σ_1, that is subvertical (vertical lithostatic stress orientation, S_v), together with the intermediate stress axis σ_2 (maximum horizontal compression orientation, S_{Hmax}) and the minimum stress axis σ_3 (minimum horizontal compression orientation, S_{hmin}) indicate a normal faulting kinematics. R = 0.15 is very low and indicates that in the first 10 km of depth, in the southwestern Gargano, σ_1 and σ_2 have similar values, greater than σ_3 (Fig. 4).

G2 Group. The stress field was inferred from the inversion of the 15 best fault plane solutions. The 95% confidence regions of the solution don't overlap and the very low misfit = 3.03° indicate homogeneity of the medium. The subvertical axis of minimum compression σ_3 (S_v) and the sub-horizontal stress axes σ_1 (S_{Hmax}) and σ_2 (S_{hmin}) indicate a thrust faulting kinematics. R = 0.3 indicates that deeper in the crust, moving toward the northeastern Gargano, the kinematics changes and s_1 and s_2 begin to differ from each other but are still greater than s_3 (Fig. 4).

G3 Group. The stress field was inferred from the inversion of 13 fault plane solutions. The 95% confidence regions of the solution don't overlap and the misfit = 4.91° indicates homogeneity of the deeper layers of the crust continuing toward northwestern in the Gargano. The subvertical axis of minimum compression σ_3 (S_v) and the sub-horizontal stress axes σ_1 (S_{Hmax}) and σ_2 (S_{hmin}) indicate a thrust faulting kinematics, like that of G2 group. R = 0.45 indicates that σ_2 has an intermediate value between σ_1 and σ_3 (Fig. 4).

G2-G3 Group. We used the events of G2 and G3 groups, that brought similar results in terms of tectonic kinematics and output parameters, to obtain a unique stress field solution. Also in this case, the 95% confidence regions of the solution don't overlap. The misfit = 5.72° represents the higher value among the considered groups, indicating a lower degree of homogeneity at depth between 15 and 25 km. The R = 0.35 is intermediate between the results of G2 and G3 groups, taken individually (Fig. 4). If we try to assemble the groups in order to include the G1 group, the results of the FMSI inversion fall outside the criteria of acceptability indicating a great heterogeneity of the focal mechanism data. In fact, if we unify the groups G1-G2, for a total of 24 focal mechanism solutions, the misfit is 6.64°; if we unify all the groups G1-G2-G3, for a total of 37 events, the misfit is 7.67°. Both the assemblages result in a misfit greater than the reference threshold of acceptability of 6°; therefore they have been both rejected.

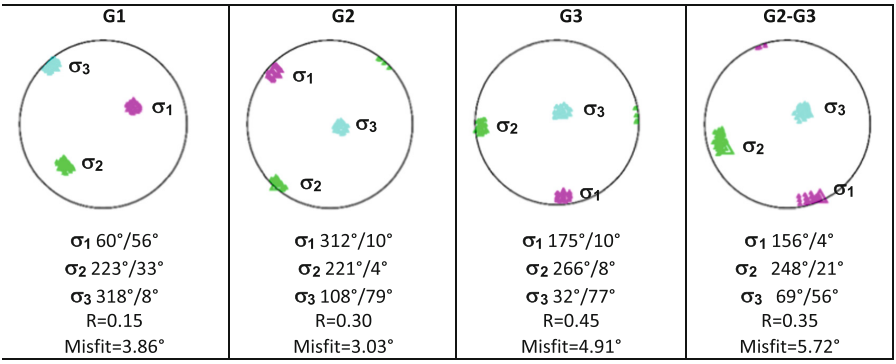


Fig. 4. Results of the FMSI inversion for the three considered event groups (G1, G2 and G3) and for the merged group G2–G3. Angles of trend/plunge of the principal stress axes (σ1, σ2, σ3) within 95% confidence area, the R value and the misfit angle are indicated for each group.

5 Discussion and Conclusions

In previous works, the lateral dependence of microearthquake foci depths (Filippucci et al. 2019a), of the coda quality factor attenuation (Filippucci et al. 2019b) and of resistivity (Tripaldi 2020) was observed. Therefore, we can hypothesize that stress field exhibits the same dependence. The focal mechanism solutions show clear variation among the considered groups: for G1 group the kinematics is normal faulting, whereas for G2 and G3 groups the kinematics is thrust faulting (Fig. 3). The composite mechanism results, obtained for the three groups separately, indicate that the solutions are stable and confirm that the kinematics of faulting changes abruptly, i.e. in few tenths of kilometers, from normal to thrust (Fig. 3). This change corresponds also to the foci deepening (Fig. 2).

The stress field results also show an abrupt change in the horizontal maximum stress direction S_{Hmax}, since it passes from normal faulting NE-SW S_{Hmax} oriented for G1 group, to a reverse faulting NW-SE S_{Hmax} oriented for the G2 and G3 groups. This indicates a clockwise rotation of S_{Hmax} moving deeper and toward the northeastern sector of the Gargano Promontory. By considering the groups G2 and G3 together, the maximum horizontal stress S_{Hmax} is oriented in an intermediate angle between the two groups taken separately.

Previous studies of focal mechanisms and stress field in this area have been proposed. Frepoli and Amato (2000), by grouping the seismicity of a broader area including the Gargano Promontory, found a normal faulting kinematics with the horizontal maximum stress oriented as for the Apennine stress (plunge/trend: σ_1 = 73/130, σ_2 = 17/310, σ_3 = 0/40). Milano et al. (2005), by analyzing the seismicity of a more restricted area (including the Gargano Promontory), found a strike-slip kinematics with an oblique (normal/strike-slip) component and the stress solution indicates normal faulting (σ_1 = 63/260 and σ_3 = 30/39). Instead, Del Gaudio et al. (2007), from the analysis of $M_L > 1.6$ seismicity, found focal mechanisms of strike-slip kinematics with a slight normal component in the southwestern zone and a slight inverse component in the northeastern promontory. Overall, they obtained a unique strike-slip stress field solution (σ_1 = 12/321, σ_2 = 55/69, σ_3 = 32/224) for the area of the Gargano Promontory. Our results for G2 and G3 groups disagree with those found by Del Gaudio et al. (2007) regarding the faulting kinematics. In fact, the strike-slip component is completely absent in our solutions. However, our results confirm the orientation of S_{Hmax} stress component found by Del Gaudio et al. (2007). This discrepancy may indicate the heterogeneity of the whole fault system. Our results do not agree with those of Milano et al. (2005) and of Frepoli and Amato (2000) in any of the areas covered by the three groups.

Considering G1 group, the kinematics is normal faulting, as characteristics of the Apennine chain, but S_{Hmax} is normal to that of the Apennine stress orientation. This result was obtained with few events and needs further investigations since, in the area covered by G1 group, the available seismic catalogues are lacking. As concern G2 and

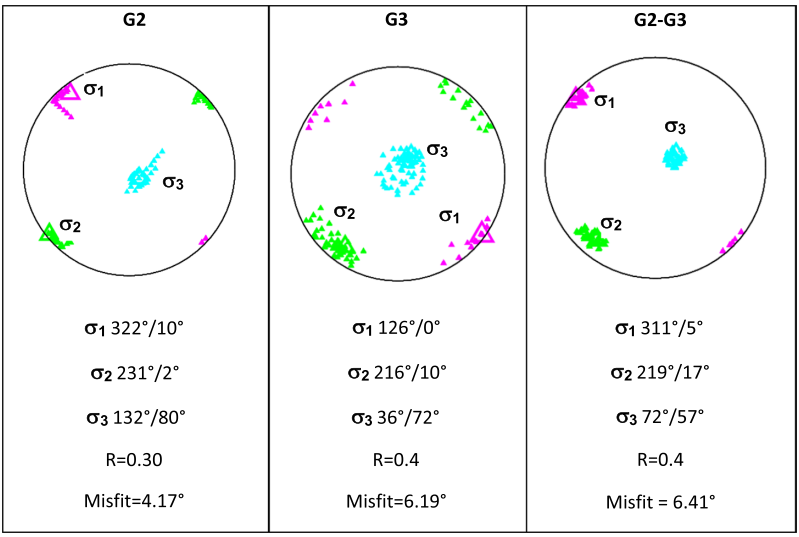


Fig. 5. Results of the FMSI inversion for the considered groups of events including the events of the dataset of Del Gaudio et al. (2007) which belong to each group. Angles of trend/plunge of the principal stress axes σ_1, σ_2, σ_3) within 95% confidence area, the R value and the misfit angle are indicated for each group

G3 groups, our results, in terms of trend and plunge of S_{Hmax}, agree with the Italian Stress Map (Montone and Mariucci 2016) even if we use a different event dataset covering a part of the Gargano Promontory, otherwise lacking information.

In order to check our results, a further inference of the stress orientation was done by adding the events of Del Gaudio et al. (2007) to our dataset. We selected only the events that fall in the volume of each group, separately. None of the events used by Del Gaudio et al. (2007) falls within the volume defined by G1 group while 4 events fall into the G2 group and 4 events into the G3 group. So, we repeated the stress inversion for the G2, G3 and for the combined G2-G3 groups (results in Fig. 5). Even if the heterogeneity of the focal mechanisms of each group increases (the misfit angle increases respect to that in Fig. 4), the results of thrust faulting are confirmed. The integration of our data with the focal mechanisms of Del Gaudio et al. (2007) indicates a slight heterogeneity of preexisting faults in the Gargano area but confirm the NW-SE thrust faulting.

The fault strike orientations in the Gargano area as inferred in this work and in the World Stress Map (WSM, Heidbach et al. 2018) disagree with the image of the surface traces of faults inferred in the area (Doglioni et al. 1994; Chilovi et al. 2000; Brankman and Aydin 2004; Patacca and Scandone 2004), indicating that the deep present-day micro-seismicity occurs on structures that are perpendicular to the mapped fault lines and to which the contractional tectonic evolution of the Gargano Promontory is attributed (Bertotti et al. 1999; Brankman and Aydin 2004; Billi et al. 2007). The disagreement between the present-day tectonic regime, as also recently sketched by Roselli et al. (2018), and the surface tectonic lines has been investigated by Billi et al.

(2007) who considered, as present-day kinematics, the normal fault regime found by Milano et al. (2005). Results however don't agree both with our study and with the WSM. So further geodynamical investigations are needed. The only way to better constrain the issues arising from this study is to pile up further events through the seismic monitoring of the Gargano area with a dense and modern seismometer array.

Acknowledgements. Figures were obtained by employing the GMT freeware package by Wessel and Smith (1998) and by the Google Earth Pro, Google, Inc. California.

Appendix

Locations of events of G1, G2 and G3groups, plotted in Fig. 3. For each event the id. number (Id), the origin (Date and Time, N Lat, E Lon and Depth), the magnitude (Ml), the residual (RMS), the horizontal and vertical errors (ERZ, ERH), the number of recording stations (Nstat), the number of recognized polarities (Npol) are reported.

G1 (Id)	Date	Time	N Lat (°)	E Lon (°)	Depth (km)	M_l	RMS (s)	ERH (km)	ERZ (km)	N_{stat}	N_{pol}
8	2013-06-28	07:02:42	41.63	15.68	3.8	0.9	0.17	0.9	1.1	8	6
11	2013-07-05	11:09:26	41.64	15.65	4.3	1.4	0.14	0.6	0.6	9	6
13	2013-07-22	12:25:47	41.64	15.65	4.6	1.5	0.16	0.6	0.8	9	6
15	2013-08-08	09:13:04	41.64	15.66	3.9	1.4	0.12	0.5	1.0	8	7
24	2013-11-25	10:12:21	41.63	15.65	4.6	1.4	0.20	0.5	1.4	9	7
34	2014-06-13	12:10:03	41.64	15.66	4.8	1.2	0.17	0.8	1.0	7	6
G2 (Id)	**Date**	**Time**	**N Lat (°)**	**E Lon (°)**	**Depth (km)**	**M_l**	**RMS (s)**	**ERH (km)**	**ERZ (km)**	**N_{stat}**	**N_{pol}**
2	2013-04-25	08:58:33	41.69	15.81	18.4	0.9	0.09	0.7	0.5	8	7
7	2013-06-25	10:02:38	41.69	15.81	18.9	1.6	0.10	0.4	0.4	11	10
11	2013-09-13	00:41:26	41.68	15.81	18.3	1.4	0.10	0.4	0.4	12	11
13	2013-09-21	03:17:42	41.71	15.79	18.5	0.4	0.09	0.5	0.4	9	8
17	2013-10-27	00:25:05	41.69	15.84	17.7	0.6	0.13	0.6	0.6	10	6
19	2013-12-08	13:13:33	41.66	15.86	12.7	0.7	0.11	0.5	0.6	9	7
20	2013-12-09	21:29:22	41.67	15.85	17.5	0.6	0.07	0.4	0.4	9	9
22	2014-01-23	14:20:49	41.66	15.73	17.9	0.7	0.07	0.3	0.3	10	9
23	2014-01-25	15:19:04	41.66	15.73	17.9	1.6	0.07	0.3	0.3	10	10
25	2014-03-03	22:40:11	41.67	15.74	19.9	0.8	0.07	0.3	0.3	11	9
30	2014-05-15	03:50:48	41.60	15.77	13.4	1.1	0.11	0.3	0.5	12	6
31	2014-06-03	01:59:42	41.68	15.72	14.5	0.1	0.07	0.3	0.4	8	6
32	2014-06-18	12:10:01	41.69	15.73	14.5	0.7	0.20	0.1	0.1	8	6
33	2014-07-05	13:25:17	41.70	15.81	14.2	0.9	0.51	1.8	2.1	11	9
34	2014-07-09	20:20:12	41.71	15.76	18.8	0.8	0.62	3.0	3.0	9	7
G3 (Id)	**Date**	**Time**	**N Lat (°)**	**E Lon (°)**	**Depth (km)**	**M_l**	**RMS (s)**	**ERH (km)**	**ERZ (km)**	**N_{stat}**	**N_{pol}**
5	2013-06-20	06:40:22	41.71	15.82	18.6	1.4	0.11	0.6	0.5	9	7
9	2013-08-04	20:08:32	41.72	15.88	19.7	0.5	0.09	0.6	0.5	8	6
12	2013-09-11	19:08:27	41.79	15.87	23.5	1.7	0.15	0.9	0.8	11	11
14	2013-10-09	02:27:56	41.70	15.86	23.9	1.0	0.12	0.7	0.6	10	6
19	2013-11-04	18:30:40	41.77	15.84	23.3	1.3	0.12	0.7	0.5	10	6
24	2013-11-23	15:03:08	41.71	15.87	22.8	1.6	0.13	0.8	0.5	12	9
35	2014-03-10	01:03:02	41.79	15.82	24.2	1.4	0.14	0.8	0.6	13	9
41	2014-04-12	03:10:02	41.72	15.88	23.1	0.8	0.20	0.9	0.7	14	12
44	2014-07-11	10:38:28	41.79	15.87	25.1	1.3	0.23	1.2	0.8	12	7

References

Bath, M., Duda, S.J.: Earthquake volume, fault plane area, seismic energy, strain, deformation and related quantities. Ann. Geofis. **17**(3), 353–368 (1964). https://doi.org/10.4401/ag-5213

Bertotti, G., Casolari, E., Picotti, V.: The Gargano Promontory, a contractional belt. Terra Nova **11**, 168–173 (1999). https://doi.org/10.1046/j.1365-3121.1999.00243.x

Billi, A., Gambini, R., Nicolai, C., Storti, F.: Neogene-Quaternary intraforeland transpression along a Mesozoic platform-basin margin: the Gargano fault system, Adria, Italy. Geosphere **3** (1), 1–15 (2007). https://doi.org/10.1130/GES00057.1

Borre, K., et al.: The COST project in Italy: analysis and monitoring of seismogenic faults in the Gargano and Norcia areas (central-southern Apennines, Italy). J. Geodyn. **36**(1–2), 3–18 (2003). https://doi.org/10.1016/S0264-3707(03)00035-8

Brankman, C.M., Aydin, A.: Uplift and contractional deformation along a segmented strike-slip fault system: the Gargano Promontory, southern Italy. J. Struct. Geol. **26**, 807–824 (2004). https://doi.org/10.1016/j.jsg.2003.08.018

Calcagnile, G., Panza, G.F.: The main characteristics of the lithosphere-asthenosphere system in Italy and surroundings regions. Pure. appl. Geophys. **119**(4), 865–879 (1980). https://doi.org/10.1007/BF01131263

Chilovi, C., De Feyter, A.J., Pompucci, A.: Wrench zone reactivation in the Adriatic block: the example of the Mattinata fault system (SE Italy). Boll. Soc. Geol. It. **119**, 3–8 (2000)

de Lorenzo, S., Michele, M., Emolo, A., Tallarico, A.: A 1D P-wave velocity model of the Gargano promontory (southeastern Italy). J. Seismol. **21**(4), 909–919 (2017). https://doi.org/10.1007/s10950-017-9643-7

Del Gaudio, V., Pierri, P., Frepoli, A., Calcagnile, G., Venisti, N., Cimini, G.: A critical revision of the seismicity of northern Apulia (Adriatic microplate - Southern Italy) and implications for the identification of seismogenic structures. Tectonophysics **436**(1–4), 9–35 (2007). https://doi.org/10.1016/j.tecto.2007.02.013

Di Bucci, D., Mazzoli, S.: The October-November 2002 Molise seismic sequence (southern Italy): an expression of Adria intraplate deformation. J. Geol. Soc. Lond. **160**(4), 503–506 (2003)

Doglioni, C., Mongelli, F., Pieri, P.: The Puglia uplift (SE Italy): an anomaly in the foreland or the Apenninic subduction due to buckling or a thick continental lithosphere. Tectonics **13**(5), 1309–1321 (1994). https://doi.org/10.1029/94TC01501

Favali, P., Funiciello, R., Mattietti, G., Mele, G., Salvini, F.: An active margin across the Adriatic Sea (central Mediterranean Sea). Tectonophysics **219**, 109–117 (1993). https://doi.org/10.1016/0040-1951(93)90290-Z

Filippucci, M., Tallarico, A., Dragoni, M., de Lorenzo, S.: Relationship between depth of seismicity and heat flow: the case of the Gargano area (Italy). Pure. appl. Geophys. **176**(6), 2383–2394 (2019a). https://doi.org/10.1007/s00024-019-02107-5

Filippucci, M., Del Pezzo, E., de Lorenzo, S., Tallarico, A.: 2D kernel-based imaging of coda-Q space variations in the Gargano Promontory (Southern Italy). Phys. Earth Planet. Int. **297**, 106313 (2019b). https://doi.org/10.1016/j.pepi.2019.106313

Frepoli, A., Amato, A.: Spatial variation in stresses in peninsular Italy and Sicily from background seismicity. Tectonophysics **317**(1–2), 109–124 (2000). https://doi.org/10.1016/S0040-1951(99)00265-6

Gephart, J.W.: FMSI: a FORTRAN program for inverting fault/slickenside and earthquake focal mechanism data to obtain the regional stress tensor. Comput. Geosci. **16**, 953–989 (1990). https://doi.org/10.1016/0098-3004(90)90105-3

Heidbach, O., et al.: The World Stress Map database release 2016: crustal stress pattern across scales. Tectonophysics **744**, 484–498 (2018). https://doi.org/10.1016/j.tecto.2018.07.007

Imanishi, K., et al.: Depth-dependent stress field in and around the Atotsugawa fault, central Japan, deduced from microearthquake focal mechanisms: evidence for localized aseismic deformation in the downward extension of the fault. J. Geophys. Res. **116**, B01305 (2011). https://doi.org/10.1029/2010JB007900

Lu, Z., Wyss, M., Pulpan, H.: Details of stress directions in the Alaska subduction zone from fault plane solutions. J. Geophys. Res. **102**(B3), 5385–5402 (1997). https://doi.org/10.1029/96JB03666

Milano, G., Di Giovambattista, R., Ventura, G.: Seismic constraints on the present-day kinematics of the Gargano foreland, Italy, at the transition zone between the southern and northern Apennine belts. Geophys. Res. Lett. **32**, L24308 (2005). https://doi.org/10.1029/2005GL024604

Montone, P., Mariucci, M.T.: The new release of the Italian contemporary stress map. Geophys. J. Int. **205**(3), 1525–1531 (2016). https://doi.org/10.1093/gji/ggw100

Patacca, E., Scandone, P.: Identificazione e valutazione di strutture sismogenetiche. Rapporto tecnico, Convenzione ENEA - Dipartimento di Scienze della Terra Università di Pisa, Italy (2001)

Patacca, E., Scandone, P.: The 1627 Gargano earthquake (Southern Italy): identification and characterization of the causative fault. J. Seismol. **8**(2), 259–273 (2004). https://doi.org/10.1023/B:JOSE.0000021393.77543.1E

Reasenberg, P., Oppenheimer, D.: FPFIT, FPPLOT and FPPAGE: FORTRAN computer programs for calculating and displaying earthquake fault-plane solutions. USGS Open-File Rep., 85–739 (1985). https://doi.org/10.3133/ofr85739

Roselli, P., Marzocchi, W., Mariucci, M.T., Montone, P.: Earthquake focal mechanism forecasting in Italy for PSHA purposes. Geophys. J. Int. **212**(1), 491–508 (2018). https://doi.org/10.1093/gji/ggx383

Rovida, A., Locati, M., Camassi, R., Lolli, B., Gasperini, P.: Catalogo Parametrico dei Terremoti Italiani (CPTI15), versione 2.0. Istituto Nazionale di Geofisica e Vulcanologia (INGV) (2019). https://doi.org/10.13127/CPTI/CPTI15.2

Salvi, S., et al.: A multidisciplinary approach to earthquake research: implementation of a geochemical geographic information system for the Gargano site, Southern Italy. Nat. Haz. **20**, 255–278 (1999). https://doi.org/10.1023/A:1008105621134

Tondi, E., Piccardi, L., Cacon, S., Kontny, B., Cello, G.: Structural and time constraints for dextral shear along the seismogenic Mattinata Fault (Gargano, southern Italy). J. Geodyn. **40** (2–3), 134–152 (2005). https://doi.org/10.1016/j.jog.2005.07.003

Tripaldi, S.: Electrical signatures of a permeable zone in carbonates hosting local geothermal manifestations: insights for the deep fluid flow in the Gargano area (south-eastern Italy). Boll. Geof. Teor. Appl. **61**(2), 219–232 (2020). https://doi.org/10.4430/bgta0312

Valensise, G., Pantosti, D., Basili, R.: Seismology and tectonic setting of the 2002 Molise, Italy, Earthquake. Earthq. Spectra **20**, 23–37 (2004). https://doi.org/10.1193/1.1756136

Wessel, P., Smith, W.H.F.: New, improved version of Generic Mapping Tools released. Eos, Trans. Am. Geophys. Un. **79**(47), 579 (1998). https://doi.org/10.1029/98EO00426

Zoback, M.L.: First and second order patterns of stress in the lithosphere: the World Stress Map Project. J. Geophys. Res. **97**, 11703–11728 (1992). https://doi.org/10.1029/92JB00132